Nanoscale

Accepted Manuscript

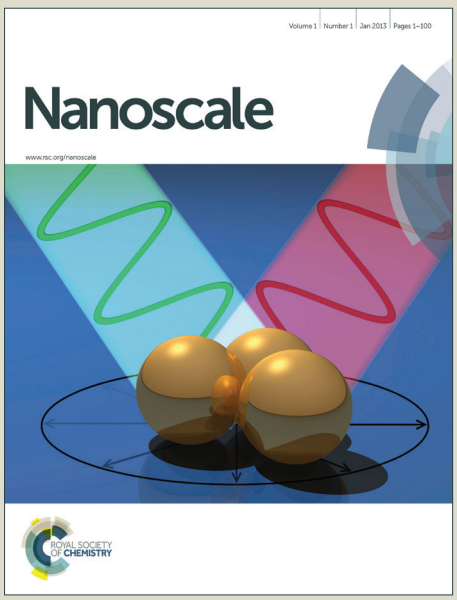

ROYAL SOCIETY OF CHEMISTRY

www.rsc.org/nanoscale

Journal Name

RSCPublishing

ARTICLE

Plasmon Mediated Shape and Size Selective Synthesis of Icosahedral Silver Nanoparticles via Oxidative Etching and Their 1-D Transformation to Pentagonal Pins

Cite this: DOI: 10.1039/x0xx00000x

R. Keunen, N. Cathcart and V. Kitaev*

Received 00th January 2012,
Accepted 00th January 2012

DOI: 10.1039/x0xx00000x

www.rsc.org/

A size- and shape-selective synthesis of pentagonally twinned silver icosahedral nanoparticles (AgI_hNPs), one of the five Platonic solid morphologies, has been developed by integrating three key factors: nuclei templating by copper, photochemical development using violet LED light and chemical oxidative etching. The presence of copper is essential for AgI_hNP shape selection via the promotion of icosahedra nuclei in precursor NPs. Violet light (401-410 nm) is crucial to promote plasmonic selection of near-spherical AgI_hNPs. Oxidative etching with hydrogen peroxide and photochemical reduction with citrate establishes a red-ox equilibrium for the photochemical selection of AgI_hNPs. The addition of chloride ions improves size- and shape-selectivity. Finally, demonstrated 1-D growth of AgI_hNPs to pentagonal pins initiated at AgI_hNP pentagonal-twinned defects highlights a universal role of twinned defects for the formation of anisotropic nanoparticles.

Introduction

Noble metal nanoparticles (MNPs) display properties distinct from bulk materials that enable unique applications[1] in sensing,[2] plasmonics[3] and catalysis.[4] Shape-selective synthesis of MNPs, such as cubes,[5] bars,[6] octahedra,[7] tetrahedra,[8] decahedra,[9] rods,[10] prisms,[11] and the realization of their advantageous properties is a current research frontier. Silver is commonly employed for NP formation due to a favorable combination of relative stability and reactivity that enables shape-selection via oxidative etching.[12] Silver is also superior for plasmonic sensing[13] and SERS applications due to its highest energy of *d*-*sp* transitions.

An icosahedron is a highly symmetric, most spherical Platonic solid.[14] Due to their pentagonal symmetry, icosahedral (I_h) MNPs must incorporate pentagonal twinned defects.[15] Icosahedra are enclosed by 20 close-packed surface facets equivalent to (111) planes and can be represented by stacking of 20 tetrahedral subunits.[16] The reported I_hMNPs are currently largely limited to palladium and gold.[10a,17-25] The majority of the reported synthetic procedures use polyols and related high temperature reactions. For the synthesis of palladium I_hNPs with well-defined facets, ethylene glycol is a common solvent, while poly(vinylpyrrolidone) (PVP) is a steric stabilizer.[16,17,19] Extensive heating at above 90 °C is typically used, and the resulting icosahedra vary in size between 25 and 50 nm.[16,17,19,20] Gold I_hNPs with the sizes ranging from 10 to 100 nm have been synthesized under conditions similar to those used for palladium icosahedra.[14,21-24] Several approaches to the synthesis of silver I_hNPs (AgI_hNPs) that require high temperatures and/or organic media have been reported.[21,26,27] Zhang et al. produced AgI_hNPs by reducing Ag^+ in 4-tert-butyl toluene at 200 °C which yielded AgI_hNPs of 9 ± 3.6 nm.[25] Kuai et al. developed an aqueous synthetic route to AgI_hNPs as large as 100 nm using PVP as a stabilizer and heating at 120 °C for 12 hrs.[21] The resulting AgI_hNPs were appreciably size-disperse with the presence of other morphologies.[21] Heterometallic I_hNPs of silver and gold have been reported to form from gold decahedral seeds upon silver addition and 8-h exposure to a halogen lamp with a band pass filter at 550 nm.[10]

The challenge created by the rounding of AgI_hNP edges that makes the morphology less distinct (and often mimicking spherical) in combination with the requirement for preservation of the regular pentagonal twinning defects results in the size- and shape-selective synthesis of AgI_hNPs not being fully addressed in the reported studies of MNPs. Shape- and size-selective icosahedral silver nanoparticles have not been reported so far, and photochemical synthesis of AgI_hNPs has not been demonstrated.

Herein we describe an aqueous, RT, shape- and size-selective synthesis of faceted AgI_hNPs with the shape yield of 95-98%. These AgI_hNPs self-assemble into regular close-packed arrays advantageous as a SERS substrate. Furthermore, we have demonstrated 1-D regrowth of AgI_hNPs at pentagonal twinned defects similar to decahedra-rod transformations.[9a,10b]

Experimental

Reagents

Silver nitrate (99%), sodium citrate tribasic dihydrate (99.5%), sodium borohydride (≥99%), hydrogen peroxide with potassium stannate inhibitor 30-32 wt%, 99.999% trace metal basis, copper(II) sulfate pentahydrate (99%), tetrachloroauric acid (99%), palladium(II) chloride (99%), palladium(II) acetylacetonate, cobalt(II) chloride hexahydrate (99%), cobalt(II) perchlorate hexahydrate, poly(sodium 4-styrenesulfonate) (PSS, M_w = 70,000), poly(acrylic acid), (PAA, M_w = 450,000), and poly(4-vinylpyridine) (M_w = 60,000) all supplied by Aldrich; and poly(vinylpyrrolidone) (PVP, M_w = 40,000) supplied by Caledon Chemicals (Caledon, Canada) were used as received. High-purity deionized water (>18.2 MΩ·cm) was produced using Millipore A10 Milli-Q.

Synthesis of Icosahedral AgNPs

In a representative AgI_hNP synthetic protocol, precursor silver NPs were first formed using a 12.7 mm by 3.2 mm stir bar spinning at ca. 90 rpm in a 20 mL vial (VWR) to mix 6.0 mL of deionized water, 0.220 – 0.270 mL of 0.05 M sodium citrate, 0 to 0.020 mL of 0.0050 M PSS, 0.090 mL of 0.0050 M silver nitrate and 0.020 mL of 0.10 M $CuSO_4$ (❶ in **Figs. 1a-c**) and lastly adding 0.230 mL of freshly prepared 0.10 M sodium borohydride to form a brown solution (❷ in **Figs. 1a-c)**. To this solution, hydrogen peroxide was added via one of three modes (see below) to produce a yellow AgNP precursor solution (❸ in **Figs. 1a-c)**. This precursor solution was exposed to a violet LED light source (**Fig S1**) for a period of 8 to 32 hrs (❹&❺ in **Figs. 1a-c**). The three modes of etching with hydrogen peroxide, each capable of producing AgI_hNPs with size and shape selectivity were as follows: 1) a single-portion addition immediately after $NaBH_4$ (0.170 mL – 0.500 mL of 10.4 M H_2O_2); 2) two-portion addition: the first after $NaBH_4$, (0.020 mL – 0.200 mL of 0.2 M or 0.190 mL of 10.4 M) and the second after a short period of exposure, ca. 30 minutes (0.020 mL – 0.225 mL of 10.4 M); and 3) three-portion addition: the first after $NaBH_4$, (0.020 mL – 0.200 mL of 0.2 M or 0.190 mL of 10.4 M), the second after a short period of exposure of ca. 30 minutes (0.020 mL – 0.225 mL of 10.4 M), and the third after overnight exposure (0.020 mL – 0.500 mL of 0.2 M) (see **Table S1**). The metal and halide dopants including $HAuCl_4$, $CoCl_2$, $PdCl_2$, and KCl were added after $CuSO_4$.

A representative size- and shape-selective AgI_hNP synthesis procedure begins with a starting volume of 6.0 mL of water and the addition of the following order of reagents to their specified final concentrations (volume and concentration of stock solutions in brackets): 1.58 mM sodium citrate (0.220 mL of 0.050 M), 0.064 mM $AgNO_3$ (0.090 mL of 0.0050 M), 0.29 mM $CuSO_4$ (0.020 mL of 0.10 M), 4.3 mM $HAuCl_4$ (0.060 mL of 0.50 mM), 2.72 mM $NaBH_4$ (0.190 mL of 0.10 M), and 0.595 M H_2O_2 (0.400 mL of 10.4 M) followed by exposure to a violet LED (409 nm, 1 W). See **Table S1** for the summary of experimental conditions of synthesis of shape- and size-selected AgI_hNPs.

Light Exposure Setup

1 W violet light emitting diodes (Prolight by SuperBright LED, USA) with a wavelength ranging from 365 nm to 420 nm (401 nm to 410 nm worked the best) and a luminous intensity of 395-475 mW were used as the light source for photochemical transformations. Lenses with a 30° or 40° (XR-LM, Super Bright LED, USA) angle were used to direct the light onto the bottom of vials resting on the lenses (**Fig. S1**). We have also used a 400 W metal halide lamp (Sunmaster) and varied its light intensity from ca. 0.1 to 0.5 mW/cm^2 by changing the distance from the lamp to the sample. All relevant LED and lamp spectra are provided in **Fig. S2**.

Gold Plating of AgI_hNPs

The gold coating precursor used was tetrachloroauric acid, $HAuCl_4$ in high-purity water (Millipore) with concentrations ranging from 0.05 to 0.005 mM. The amount of $HAuCl_4$ was calculated relative to the total amount of silver present in the AgI_hNPs, used for the plating. To prepare a 10 mol. % gold plating solution, 0.012 mL of 0.005 M $HAuCl_4$ was added to 3.99 mL of deionized water. Using the entire volume of the prepared AgI_hNP sample (see above), 3.0 ml of Au plating solution was dispensed over a period of 4 hrs using a syringe pump (KdScientific 220) at a rate of 0.500 mL/hr for the first 2 hrs, followed by 1.00 mL/hr for the last 2 hrs (**Fig. S3**).

1-D regrowth of AgI_hNPs to Pentagonal Pin Morphologies

AgI_hNPs were first concentrated 10 times by centrifugation of 5.00 mL of the as-prepared AgI_hNPs and replacement of the supernatant with deionized water to a total volume of 0.500 mL. The resulting silver concentration in the concentrated AgI_hNPs was 0.74 mM. In a 20 mL vial, 3.0 mL of water, 0.180 mL of 0.05 M sodium citrate, and 0.033 mL of 0.05 M PVP were heated to near boiling: 98-100 °C on a heating block set at 103-105 °C (AccuBlock Digital Dry Bath). After temperature equilibration for ca. 7-10 minutes, 0.500 mL of concentrated AgI_hNP solution was added, followed by silver nitrate one minute later. The amounts of added silver nitrate were varied between 0.270 mL and 0.540 mL of 0.0050 M solution. After addition of silver nitrate, the reaction continued to be heated for 8 to 30 minutes.

Characterization

Electron microscopy (EM) both transmission (TEM) and scanning (SEM) was performed using Hitachi S-5200. NP solutions were deposited on a carbon-coated Formvar grid (EMS Corp.). Operating voltage was 30.0 kV. The average size and standard deviation were determined from SEM and TEM images using the data for at least 100 particles. UV-vis spectra were acquired with either Ocean Optics QE65000 fiber-optic or Cary 50Bio UV-vis spectrophotometers. Raman spectra were recorded using an R-3000QE fiber-optic Raman spectrometer equipped with a 290 mW laser at 785 nm (RSI), operated at 190–210 mW with typical spectral acquisition time of 5 seconds.

Results and discussion

Shape- and size- selective synthesis of AgI_hNPs has been successfully accomplished by a multistage single-batch process, summarized in the schematics of **Figs. 1a**,**b**. Representative optical spectra and electron microscopy images of the prepared AgI_hNPs are shown in **Fig. 1c** and **Figs. 1d-f**, **Fig. 2** and **Fig. 3**, respectively. AgI_hNPs with a range of SPR maxima from 420 to 455 nm (**Fig. S4**), corresponding to average diameters of 45 nm to 65 nm, 5-8% standard size deviation, and shape yield of 95-98% have been achieved.

The AgI_hNP synthesis starts with the reduction of silver nitrate by sodium borohydride in the presence of citrate, Cu^{2+} ions and PSS to form a mixture of few-atom cluster species[28,29] and small nanoparticles (❷ in **Figs. 1a-c**). Hydrogen peroxide is then added as an oxidizing agent to establish a red-ox equilibrium and to initiate formation of larger silver nanoparticle nuclei (❸ in **Figs. 1a-c**). This coarse mixture of AgNPs serves as a precursor for photochemical transformation via exposure to violet LEDs. Due to the considerable intricacy of the AgI_hNP synthesis, we first discuss key reagents and parameters and then all individual factors in more detail.

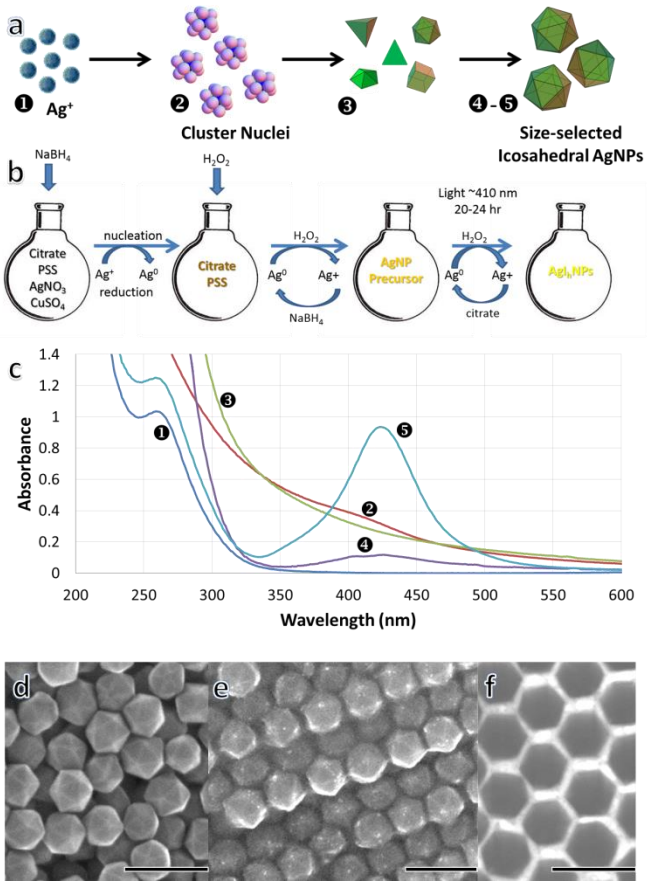

Figure 1. Development stages of AgI_hNPs. **a)** Schematics showing the growth and refinement of the AgNPs. **b)** Schematics illustrating the order of reagent addition and corresponding transformations. **c)** Representative UV-vis spectra for development stages of AgI_hNPs: ❶ before addition of $NaBH_4$; ❷ after addition of $NaBH_4$ ❸ after addition of H_2O_2; ❹ after 5 min of light exposure; ❺ after 19 hrs of exposure. **d)-f)** Representative electron microscopy (EM) images of AgI_hNP faceting (**d**)) and close-packed layers of AgI_hNPs (**e)-f)**). All scale bars are 100 nm.

Key Factors in AgI_hNP Synthesis

Together with silver ions and borohydride, citrate, Cu^{2+}, hydrogen peroxide and exposure to violet light (395 nm to 420 nm) are the key components for the synthesis of shape- and size-selected AgI_hNPs. In addition, chloride and tetrachloroaurate are beneficial for shape selectivity and faceting.

In absence of Cu^{2+} in the synthesis, poorly shaped quasi-spherical particles become the main product (**Fig. S5A**). In absence of light development, the reaction outcome is a crude mixture of small nanoparticles (❸ in **Fig. 1a**) or total dissolution of nanoparticles at higher peroxide concentrations. Violet light directs growth of isotropic particles and favors the selection of stable highly symmetric AgI_hNPs (❹-❺ in **Figs. 1a-c**) in appropriate red-ox conditions, where the oxidation is accomplished by peroxide and photochemical reduction by citrate.[30]

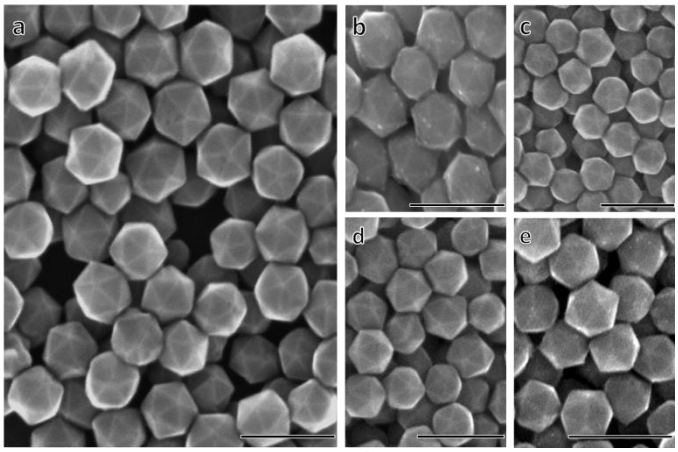

Figure 2. Representative SEM images of prepared AgI_hNPs. All scale bars are 100 nm.

Citrate plays a multifunctional role in the system: serving in charge stabilization, as a ligand directing formation of (111) Ag facets,[31] & as a reducing agent in photochemical transformations.[30] H_2O_2 (or similar oxidizers) is essential to establish a red-ox equilibrium that drives AgI_hNPs shape selection in the conditions favoring the selective growth of icosahedral seeds (**Fig. S5B**).

For steric stabilization, we have realized that commonly used poly(vinylpyrrolidone) (PVP) is too protective and deteriorates shape selection (see **Fig. S6B,E**). Weaker binding polymers, such as poly(sodium 4-styrenesulfonate), were found to work better (**Fig. S6C,D)**. Ultimately, synthetic conditions were established to exclude sterically stabilizing polymers from AgI_hNP synthesis (**Fig. S6A** and **Figs. 2,3**); see Table S1 for specific details.

Copper and Other Metal Dopants

Presence of Cu^{2+} was found to be essential for the formation of size- and shape-selected AgI_hNPs. EM images of **Figs. S5A** and **S7C** illustrate size-disperse polyhedral quasi-spherical AgNPs with only a small fraction of well-faceted AgI_hNPs in the absence of copper. The critical role of copper in the system was elucidated by testing several other metal ions instead of copper (Pd(II) (**Fig. S7A**), Fe(III) (**Fig. S7B**), and Co(II) (**Fig. S7D**)). Different metal ions resulted in smaller misshapen nanoparticles and platelets, polyhedral NPs, and large platelets respectively. Furthermore, the role of other metals used in combination with copper was examined. Co(II) (**Fig. S8B**) was found to produce better results than Pd(II) (**Fig. S8A**) and other metals. See **SI** for more information.

Our initial hypothesis for copper's essential role was related to the icosahedral core geometry. To form a perfect close packed structure for the smallest icosahedral nucleus of 13 atoms, the diameter of the central atom should be ca. 85% of the surrounding 12 atoms. This bodes well for the copper atom fitting into the centre of the silver icosahedral core, since metallic radii of copper and silver are 0.128 nm and 0.144 nm, respectively. However, in light of the recent convincing evidence that the stable icosahedral core of silver clusters is hollow,[32,33] a more likely scenario is that copper first participates in the formation of the cluster nuclei being reduced by borohydride in the very first stage of the synthesis (❶-❷ in **Fig. 1a-c**). Subsequently, in the oxidative conditions, upon addition of hydrogen peroxide to a precursor mixture of small clusters and nanoparticles, Cu atoms are likely eliminated (the redox potential of copper is substantially lower than silver) leaving hollow icosahedral nuclei. This scenario can explain reasonably well the relatively high copper concentration required to promote icosahedral cores. The reduction of copper alone (in absence of silver while otherwise identical conditions of AgI_hNP precursor formation) is demonstrated in **Fig. S9**. Copper clusters (small NPs) survive for ca. 4 hrs in absence of hydrogen peroxide (**Fig. S9**), while dissolving immediately upon peroxide addition. Cluster formation upon initial reduction is largely a stochastic process: only a very small fraction of stable icosahedral clusters that form subsequently grow at the expense of other less stable species.

It is also feasible that Cu^{2+} plays a role in enhancement of the redox equilibrium as Cu(I)/Cu(II) in conjunction with borohydride and peroxide.[34]

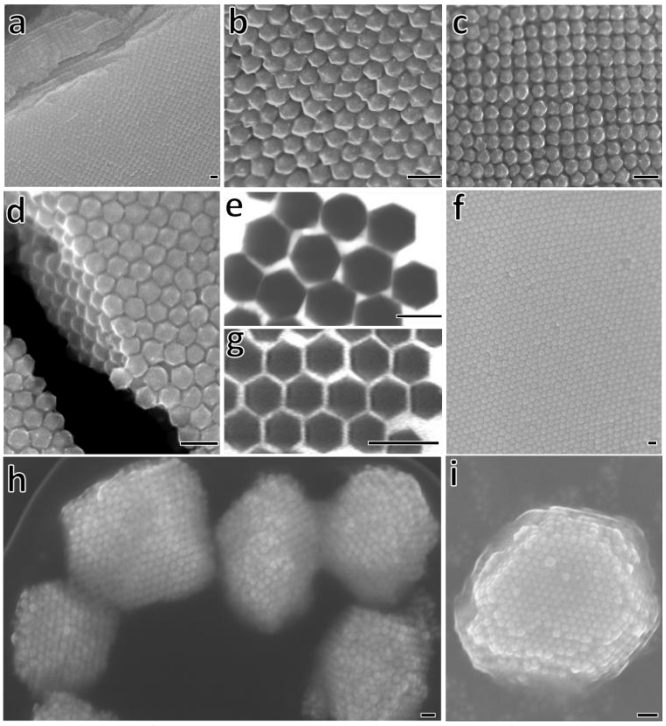

Figure 3. a)-d), f) SEM images and **e), g)** TEM images of the close-packed assemblies of AgI_hNPs. **h)** and **i)** SEM images of close-packed crystals of AgI_hNPs. All scale bars are 100 nm.

Light Exposure

Photochemical transformation of a AgNP precursor mixture containing icosahedral seeds in oxidative conditions is the key stage of the AgI_hNP synthesis. Without light exposure, no precursor development can take place since citrate does not function as an effective reducing agent at RT in absence of plasmonic excitation.[30] In contrast, thermal development either produces large platelets (**Fig. S10**) or leads to complete AgNP dissolution.

The relevant LED and lamp spectra are given in **Fig. S2**. Half width at half maxima (HWHM) values for LED emission are 4-8 nm which are suitable for efficient shape and size selection through selective plasmonic excitation and growth.[10a,36]

Violet light is instrumental for selective growth of icosahedral seeds from the precursor mixture. The primary reason for this role is that the wavelength range of 395-420 nm corresponds to the transverse SPR of anisotropic silver nanoparticles, such as rods,[10b, 35] prisms,[11a,b,31] and decahedra.[9] Specifically, this transverse for decahedral NPs with the diameters of 30-60 nm is at ca. 400-420 nm. At the same time, near-spherical icosahedra feature only a

single SPR peak that for larger AgI_hNPs (ca. >30 nm in diameter) can occur at more than 420 nm and thus shift away from the LED excitation upon AgI_hNP growth. As a result, icosahedral particles can grow and become stable while that is not the case for anisotropic particles, including decahedra, which are kept constantly excited and ultimately dissolve in the conditions of the red-ox equilibrium.

For the wavelength of LED exposure, the range from 401 nm to 410 nm was found to be most effective. The conditions of the photochemical growth were fine-tuned predominantly for 406-409 nm LEDs, though AgI_hNP formation with 401 nm light worked as well (**Table S1**, **Fig. 4a**). Exposure of the precursor AgNP solution to light of longer wavelengths (>417 nm) results in increasing formation of decahedra (spectrum ❹ in **Fig. 4a,c** and **Fig. S11)**. At even longer exposure wavelength (>505 nm), platelets become a dominant product.[35,36]

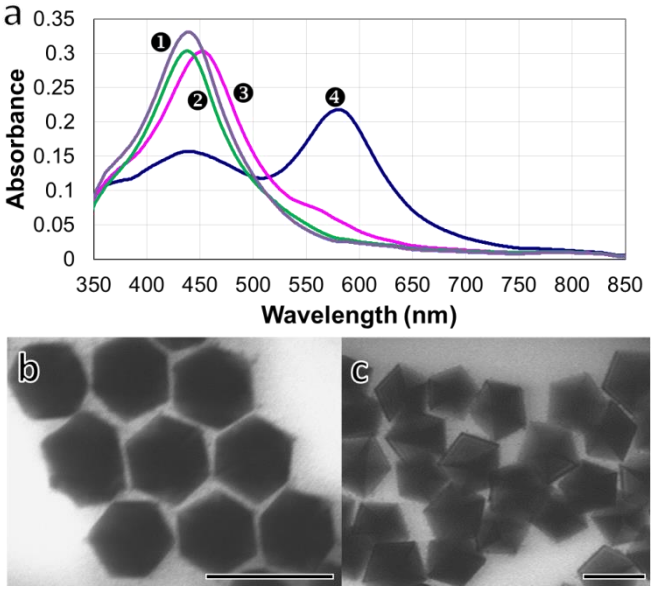

Figure 4. Effect of LED wavelength on the development of AgI_hNP precursors. **a)** UV-vis spectra of samples developed upon exposure to LED with emission maxima at: ❶ 401 nm; ❷ 404 nm; ❸ 410 nm; ❹ 417 nm. TEM images of samples prepared by exposure to **b)** 410 nm LED light. **c)** 417 nm LED light. All scale bars are 100 nm.

Other than icosahedra, morphologies that can develop from the precursor solution include decahedral, octahedral, and planar-twinned AgNPs (platelets, prisms). Icosahedra, decahedra and octahedra are established as three primary, stable core nuclei of small gold and silver clusters.[37] We have not observed octahedral AgNPs since their corresponding nuclei are stable at larger size ranges not accessible in our experimental conditions, while our precursor AgNP solution formed from small (few atoms) clusters that correspond to the stability range of icosahedral and decahedral cores.[37] Decahedral AgNPs were indeed the prominent impurity that had to be carefully minimized in our AgI_hNP synthesis. Competing planar twinned morphologies form by fast kinetic growth[11a,] and become a predominant product in conditions where photochemical growth is hampered (e.g. in thermal treatment (**Fig. S10**) or in presence of less reactive metals, such as Pd^{2+} (**Fig. S7A**)).

Further details on the effect of intensity, exposure times and different light sources are described in **SI**.

Development Stages of AgI_hNP Synthesis

AgI_hNP formation proceeds through several distinct stages (**Fig. 1a,b**) that can be monitored by UV-vis spectroscopy (**Fig. 1c** and **Fig. S12**). Upon addition of the reducing agent ($NaBH_4$), the solution rapidly changes from colourless (❶ in **Fig. 1c**) first to pale yellow and then to brown (❷ in **Fig. 1c**). The brown colour is indicative of the presence of a mixture of clusters and small undefined AgNPs with their characteristic broad absorbance at 400 to 500 nm.

After hydrogen peroxide is added, the reaction colour quickly changes to deep yellow (❸ in **Fig. 1c** & ❶ in **Fig. S12**) that is characteristic of the formation of small plasmonic AgNPs. The onset of the AgI_hNP development occurs after only ca. 5 min of light exposure (❷ in **Fig. S12**). After few hours of exposure (**Fig. S12)**, an appreciable population of AgI_hNPs with the limited size uniformity (**Fig. S13)** is present. Complete conversion is typically reached in 14-21 h (**Fig. S12**). All silver remains in a metallic form during the photochemical exposure due to the citrate serving as a reducing agent.

Oxidative Etchants: H_2O_2 and Persulfate

Oxidative etchants are instrumental for the shape selection that enables selective growth of AgI_hNPs at the expense of other less stable AgNPs in the regrowth conditions: violet light exposure in our case. The primary role of an oxidative etchant is to establish a red-ox equilibrium by dissolution of less stable AgNP entities. The resulting equilibrium is delicate for AgNP formation in general and is particularly sensitive in the case of AgI_hNPs with a very narrow range of suitable etching conditions.

Hydrogen peroxide is one of the common oxidative etchants in AgNP synthesis given its versatility of use and conversion to water.[11] Without hydrogen peroxide or other oxidative etchants, photochemical shape selection in the system cannot be achieved (**Fig. S5B**). In the absence of both hydrogen peroxide and light exposure, the AgNP seeds develop into a mixture of different clusters and NPs (❷ in **Fig. 1c**). When larger amounts of H_2O_2 are used, the etching dominates and causes complete dissolution of AgNPs.

The most successful way of etching in AgI_hNP synthesis was with hydrogen peroxide added in several (typically two) portions at different points during the AgI_hNP growth. By this method, smaller particles were largely eliminated from the final AgI_hNPs. More details on different etching experiments performed and successful replacement of hydrogen peroxide with persulfate (**Fig. S5B,C**) are given in **SI**.

Chloride Role in Enhanced Etching

Chloride was found to serve as an effective co-etchant that significantly improved AgI_hNPs size selection, especially decreasing the amount of smaller icosahedral and quasi-spherical AgNPs. The optimal chloride concentration in the system was found to be ca. 18 μM (375:1 molar ratio of silver to chloride). We have also found that chloride was more effective as a part of complex ions, such as cobalt chloride and tetrachloroaurate, likely due to bound chloride ions serving as a milder etchant. The role of chloride as an etchant in combination with oxygen was greatly elucidated by the work of Younan Xia's group.[2a,6b] In the developed AgI_hNP synthesis with hydrogen peroxide as a main etchant, chloride is not essential but

beneficial for the synthesis (**Table S1**) and can also be used in post-synthetic transformations as described in **SI** (**Fig. S14**).

$HAuCl_4$ as a Dopant

The primary effect of small amounts of tetrachloroaurate is due to its constituent chloride ions. In the absence of Cu^{2+}, Au^{3+} cannot enhance the synthesis of AgI_hNPs similarly to the other metals (**Fig. S15B).** Larger amounts of $HAuCl_4$ (starting form ca. 29 μM or a molar ratio of 2.25 Ag to 1 Au), inhibits the growth of AgNPs (**Fig. S15A**) due to gold inertness similar to palladium. Smaller amounts of $[AuCl_4]^-$ (optimally at ca. 15:1 Ag/Au molar ratio) were helpful to improve the size-selection and also to enhance the ability of the resulting AgI_hNPs to self-assemble into close-packed arrays (**Fig. 3**). At the same time, the presence of gold led to less defined AgI_hNP facets (**Figs. 2a,b,e**). Another effect of gold doping was the SPR shift of AgI_hNPs by ca. 15-20 nm (**Fig. S16, Table S1**).

Effect of Bromide and Iodide

The effect of bromide on the synthesis of AgI_hNPs was entirely detrimental both when it was added at the initial development stage (arresting the growth, **Fig. S17B**) and upon photochemical transformation (AgNPs became less stable in presence of bromide and dissolved). Similarly, iodide addition did not have any beneficial effect, leading to more rounded particles without noticeable changes in AgI_hNP size-selectivity, even at very low iodide concentration of 0.40 nM (**Fig. S17A**).

Effect of Sterically Stabilizing Polymers

Sterically stabilizing polymers, such as PVP, are commonly used in AgNP synthesis to improve stability by minimizing aggregation. Our first-generation AgI_hNP synthesis employed PVP (**Figs. S6B,E**). Subsequently, it was realized that weaker binding polymers, such as PSS are superior for better AgI_hNP size- and shape- selection (**Figs. S6C,D**). We have also tested poly(4-vinylpyridine), and poly(acrylic acid); their effects are described in SI. Initial attempts of polymer removal in AgI_hNP synthesis were not successful due to the delicate balance of oxidation conditions required for photochemical transformations; however, a synthetic protocol without sterically stabilizing polymers has been ultimately successfully developed (**Figs. 2**, **3, S6A**, and **Table S1**).

Other Factors

Effects of silver concentration, reducing agents (including ascorbic acid), pH, and stirring conditions on this highly sensitive AgI_hNP synthesis are elaborated in **SI**.

Self-Assembly of AgI_hNPs into Close Packed Lattices

Achieving high levels of AgI_hNP size-selectivity (ca. 5-8% standard deviation) enabled their self-assembly into close packed arrays (**Fig. 3**) similar to those observed for monodisperse spherical particles. Close-packed arrays of AgI_hNPs also tended to form microscopic crystals that often preserved the pentagonal symmetry of constituent NPs (**Figs. 3h,i**).

High-quality uniform close-packed arrays of AgI_hNPs can be advantageous for SERS, given the formation of the uniform cavities in the periodic arrays surrounded by well-defined polygonal facets. As a proof of concept, we have demonstrated reliable detection (S/N=3) of 50 pmole of thiosalicylic acid using dry close-packed AgI_hNP arrays as a substrate. A corresponding SERS spectrum is shown in **Fig. S18**. Consequently, size-selected, faceted AgI_hNPs are promising for SERS, given their propensity to self-assemble into regular close packed arrays and size tuning achievable by this synthesis.

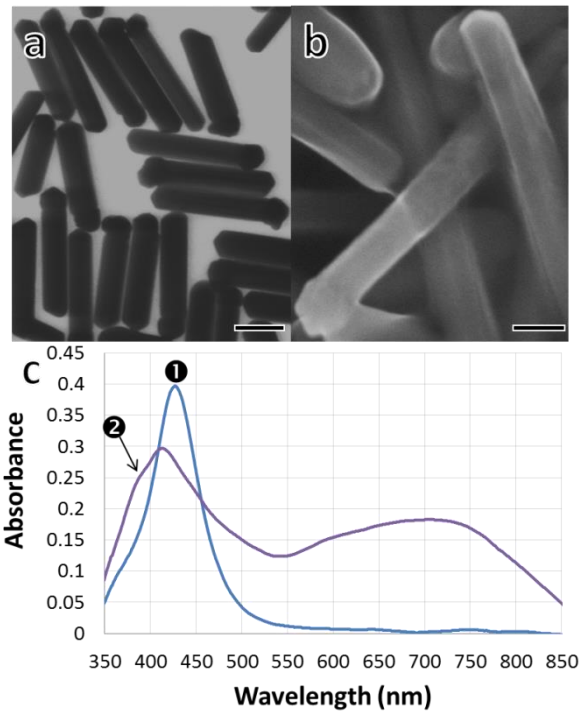

Figure 5. 1-D regrowth of AgI_hNPs. **a)** TEM and **b)** SEM images of the resulting silver pentagonal pins. **c)** UV-vis spectra of ❶ precursor AgI_hNP and ❷ regrown pentagonal pins. All scale bars are 100 nm.

1-D Regrowth of AgI_hNPs at Pentagonal Twinned Defects: Formation of Pentagonal Pins

Using a synthetic protocol reported for the growth of pentagonal rods from decahedral AgNPs,[10b] we developed the regrowth of AgI_hNPs into pentagonal rod-like morphologies that bear close similarity to pins due to their icosahedral heads (**Figs. 5a,b**). Pentagonal facets of the pins are demonstrated in **Fig. S19**. 1-D growth is initiated from one of the pentagonal twinned facets leaving the spherical-like "head" of rounded icosahedra on the resulting pentagonal pins (**Figs. 5a,b**). Spectrum ❶ in **Fig. 5c** corresponds to precursor AgI_hNPs used to regrow the pentagonal pins shown in **Figs. 5a,b**. Spectrum ❷ in **Fig. 5c** features two peaks at ca. 400 nm and 700 nm that are characteristic of two SPR modes common to Ag nanorods: transverse and longitudinal, respectively.[35]

The demonstrated 1-D growth of AgI_hNPs is important evidence that the anisotropic rod formation is primarily defect-driven. The growth is initiated at the gap of the pentagonal twinned defects,[10b] which are present as a result of the incompatibility of the pentagonal symmetry with the symmetry of the fcc lattice of silver. Further work is in progress to test the formation of multiple rods from the same icosahedral seeds.

Conclusions

In summary, the synthesis of size- and shape- selected AgI_hNPs capable of self-assembly into close-packed arrays has been

developed. The role of multiple synthetic parameters including the light wavelength, intensity, and exposure time, concentrations of silver, reducing agents, copper and other metal dopants, sterically stabilizing polymers, and etchants has been elucidated. Finally, 1-D regrowth of AgI_hNPs to pentagonal pins initiated at one of the pentagonally twinned faces has been demonstrated.

Acknowledgements

The authors are grateful to NSERC, the Government of Ontario (ERA), and Wilfrid Laurier University (URA) for financial support. Ilya Gourevich and Neil Coombs (Centre for Nanostructure Imaging, University of Toronto) are acknowledged for support with electron microscopy imaging.

Keywords: silver nanoparticles, icosahedra, pentagonal twinned defects, shape- and size-selection, oxidative etching, photochemical synthesis, 1-D growth, pentagonal pins

Notes and References

[a] Department of Chemistry, Wilfrid Laurier University, 75 University Ave. W., Waterloo, Ontario, Canada N2L 3C5 email: vkitaev@wlu.ca

Electronic Supplementary Information (ESI) available: additional information on synthetic series. See DOI: 10.1039/b000000x/

[1] a) S. Eustis, M. El-Sayed, *Chem. Soc. Rev.* 2006, **35**, 209-217. b) T. K. Sau, A. L. Rogach, F. Jäckel, T. A. Klar, J. Feldmann, *Adv. Mater.* 2010, **22**, 1805-1825.

[2] a) Y. Xia, W. Li, C. M. Cobley, J. Chen, X. Xia, Q. Zhang, M. Yang, E. C. Cho, P. K. Brown, *Acc. Chem. Res.* 2011, **44**, 914-924. b) A. M. Alkilany, S. E. Lohse, C. J. Murphy, *Acc. Chem. Res*. 2013, **46**, 650-661.

[3] a) Q. Gan, F. J. Bartoli, Z. H. Kafafi, *Adv. Mater*. 2013, **25**, 2385-2396. b) J. B. Pendry A. Aubry, D. R. Smith, S. A. Maier, *Science* 2012, **337**, 549-552.

[4] a) M. A. Mahmoud, R. Narayanan, M. A. El-Sayed, *Acc. Chem. Res.* 2013, **46**, 1795-1805. b) W. B. Hou, S. B. Cronin, *Adv. Funct. Mater*. 2013, **23**, 1612-1619.

[5] a) M. L. Personick, M. R. Langille, J. Zhang, J. Wu, S. Li, C. A. Mirkin, *Small* 2013, **9**, 1947-1953. b) J. Zhang, J. Fang, *J. Am. Chem. Soc*. 2009, **131**, 18543-18547. c) M. McEachran, V. Kitaev, *Chem. Commun*. 2008, **44**, 5737-5739.

[6] a) Y. Xiong, H. Cai, B. J. Wiley, J. Wang, M. J. Kim, Y. Xia, *J. Am. Chem. Soc*. 2007, **129**, 3665-3675. b) B. J. Wiley, Y. Chen, J.M. McLellan, Y. Xiong, Z-Y. Li, D. Ginger, Y. Xia, *Nano Lett*. 2007, **4**, 1032-1036.

[7] a) Y. Wang, S. Xie, J. Liu, J. Park, C. Z. Huang, Y. Xia, *Nano Lett*. 2013, **13**, 2276-2281. b) J. Zhang, Y. Gao, R. A. Alvarez-Puebla, J. M. Buriak, H. Fenniri, *Adv. Mater*. 2006, **18**, 3233-3237.

[8] G. Fu, X. Jiang, L. Ding, L. Tao, Y. Chen, Y. Tang, Y. Zhou, S. Wei, J. Lin, T. Lu, *Appl. Catalysis B* 2013, **138-139**, 167-174.

[9] a) B. Pietrobon, V. Kitaev, *Chem. Mater*. 2008, **20**, 5186-5190. b) X. Zheng, X. Zhao, D. Guo, B. Tang, S. Xu, B. Zhao, W. Xu, J. R. Lombardi, *Langmuir* 2009, **25**, 3802-3807.

[10] a) M. R. Langille, J. Zhang, C. A. Mirkin, *Angew. Chemie Int. Ed.* 2011, **50**, 3543-3547. b) B. Pietrobon, M. McEachran, V. Kitaev, *ACS Nano* 2009, **3**, 21-26.

[11] a) N. Cathcart, A.J. Frank, V. Kitaev, *Chem. Commun*. 2009, **46**, 7170-7172. b) N. Cathcart, V. Kitaev, *ASC Nano* 2011, **5**, 7411-7425. c) N. Cathcart, V. Kitaev, *Nanoscale* 2012, **4**, 6981-6989.

[12] Y. Sun, Y. Xia, *Science* 2002, **298**, 2176-2179.

[13] B. Sepúlveda, P. C. Angelomé, L. M. Lechuga, L. M. Liz-Marzán, *Nano Today* 2009, **4**, 244-251.

[14] a) F. Kim, S. Connor, H. Song, T. Kuykendall, P. Yang, *Angew. Chem. Int. Ed.* 2004, **43**, 3673-3677. b) W. Niu, G. Xu, *Nano Today* 2011, **6**, 265-285.

[15] J. Montejano-Carrizales, J. L. Rodriguez-Lopez, U. Pal, M. Miki-Yoshida, M. Jose-Yacaman, *Small* 2006, **2**, 351-355.

[16] a) Y. Xiong, J. McLellan, Y. Yin, Y. Xia, *Angew. Chem. Int. Ed.* 2007, **119**, 804-808.b) M. R. Langille, J. Zhang, M. L. Personick, S. Li, C. A. Mirkin, *Science* 2012, **337**, 954-957.

[17] D. Seo, C. I. Yoo, I. S. Chung, S. M. Park, S. Ryu, H. Song, *J. Phys. Chem. C* 2008, **112**, 2469-2475.

[18] Y. Chen, B. He, T. Huang, H. Liu, *Colloids Surf. Physicochem. Eng. Aspects* 2009, **348**, 145-150.

[19] C. Li, R. Sato, M. Kanehara, H. Zeng, Y. Bando, T. Teranishi, *Angew. Chem. Int. Ed.* 2009, **48**, 6883-6887.

[20] B. Lim, Y. Xiong, Y. Xia, *Angew. Chem. Int. Ed.* 2007, **46**, 9279-9282.

[21] L. Kuai, B. Geng, S. Wang, Y. Zhao, Y. Luo, H. Jiang, *Chem. Eur. J.* 2011, **17**, 3482-3489.

[22] M. Yavuz, W. Li, Y. Xia, *Chem. Eur. J.* 2009, **15**, 13181-13187.

[23] W.-K. Lee, S.-H. Cha, K.-H. Kim, B.-W. Kim, J.-C. Lee, *J. Sol. State Chem.* 2009, **182**, 3243-3248.

[24] K. Kwon, K. Y. Lee, Y. W. Lee, M. Kim, J. Heo, S. J. Ahn, S. W. Han, *J. Phys. Chem. C* 2007, **111**, 1161-1165.

[25] Q. Zhang, J. Xie, J. Yang, J. Y. Lee, *ACS Nano* 2009, **3**, 139-148.

[26] C. R. Li, N. P. Lu, Q. Xu, J. Mei, W. J. Dong, J. L. Fu, Z. X. Cao, *J. Cryst. Growth* 2011, **319**, 88-95.

[27] M. Tsuji, M. Ogino, R. Matsuo, H. Kumagae, S. Hikino, T. Kim, S. Yoon, *Crystal Growth & Design* 2010, **10**, 296-301.

[28] M. Walter, J. Akola, O. L. Acevedo, P. D. Jadzinsky, G. Calero, C. J. Ackerson, R. L. Whetten, H. Gronbeck, H. Hakkinen, *PNAS* 2008, **105**, 9157-9162.

[29] N. Cathcart, P. Mistry, C. Makra, B. Pietrobon, N. Coombs, M. Jelokhani-Niaraki, V. Kitaev, *Langmuir* 2009, **25**, 5840–5846.

[30] X. Wu, P. L. Redmond, H. Liu, Y. Chen, M. Steigerwald, L. Brus, *J. Am. Chem. Soc.* 2008, **130**, 9500-9506.

[31] C. Xue, G. S. Metraux, J. E. Millstone, C. A. Mirkin, *J. Am. Chem. Soc.* 2008, **130**, 8337-8344.

[32] A. Desireddy, B.E. Conn, J. Guo, B. Yoon, R. N. Barnett, B. M. Monahan, K. Kirschbaum, W. P. Griffith, R. L. Whetten, U. Landman, T. P. Bigioni, *Nature* 2013, **501**, 399–402.

[33] H. Yang, Y. Wang, H. Huang, L. Gell, L. Lehtovaara, S. Malola, H. Häkkinen, N. Zheng, *Nat. Commun*. 2013, **4**, #2422, DOI: 10.1038/ncomms3422.

[34] M. J. Mulvihill, X. Y. Ling, J. Henzie, P. Yang, *J. Am. Chem. Soc*. 2010, **132**, 268–274.

[35] N. Murshid, D. Keogh, V. Kitaev, *Part. Part. Syst. Charact*. 2014, **31**, 178-189.

[36] K. G. Stamplecoskie, J. C. Scaiano, *J. Am. Chem. Soc.* 2010, **132**, 1825−1827.

[37] C. L. Cleveland, U. Landman, *J. Chem. Phys*. 1991, **94**, 7376-7396.

Journal Name RSCPublishing

ARTICLE